Supporting Information

Motor and Rotor in One: Light-Active ZnO/Au Twinned Rods of Tunable Motion Modes

Sinan Du,[†,#] Huaguang Wang,[#] Chao Zhou,[‡] Wei Wang,[‡,*] Zexin Zhang [#,†,*]

[†] Center for Soft Condensed Matter Physics and Interdisciplinary Research, Soochow University, Suzhou 215006, China

[#] College of Chemistry, Chemical Engineering and Materials Science, Soochow University, Suzhou 215123, China

[‡] School of Materials Science and Engineering, Harbin Institute of Technology (Shenzhen), Shenzhen 518055, China

1. Supporting Videos

Videos were recorded at 10 frames per second by a Basler ACE camera fitted on a Zeiss Observer A1 microscope. And here the supporting videos are played back at 5 times their original speeds to help illustrate the dynamics.

1. **Video S1**, showing the effect of H_2O_2 concentrations on the modes of motion of the ZnO/Au rods (AVI format).

2. **Video S2**, showing the orientation of incident light dictates the modes of motion of the ZnO/Au rods (AVI format).

2. Supporting Figures

2.1 Further characterizations of the ZnO/Au rods

We measured 120 ZnO/Au rods and found that the rods are uniform in length, which is 3.3 ± 0.2 μm. The equivalent diameters of the hexagonal cross-sections of the two segments are 1.5 ± 0.1 μm and 1.6 ± 0.1 μm, respectively.
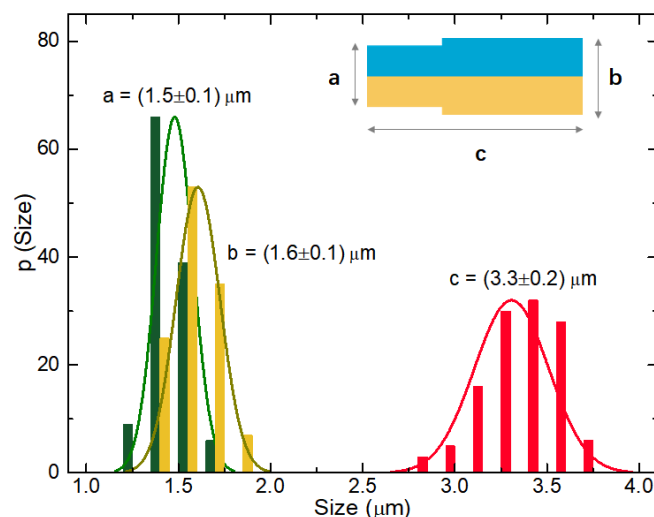

Figure S1. Size distribution of ZnO/Au rods. The geometrical information of a rod is shown in the inset.

X-ray powder diffraction (XRD) patterns confirm the purity and crystalline properties of the ZnO rods (Figure S2a). All diffraction peaks can be indexed as Wurtzite structure (hexagonal phase), which agrees well with the Joint Committee on Powder Diffraction Standard card (JCPDS 36-1451).[1, 2] The sharp diffraction peaks and the lack of impurity peaks indicate the excellent crystallinity of the as-synthesized ZnO rods. Then Janus ZnO/Au rods were fabricated by sputtering Au onto a monolayer of the ZnO rods deposited on a glass slide. The effect of sputtering Au on the crystal structure of ZnO was again evaluated by XRD (Figure S2b). New characteristic peaks marked by triangles appear, which can be assigned to the metallic Au (JCPDS 04-0784).[2] Thus the XRD results confirming the successful introduction of Au on the surface of the ZnO rod. The energy-dispersive X-ray (EDX) results further confirm the Janus structure of the ZnO/Au rod (Figure S3b-3d).
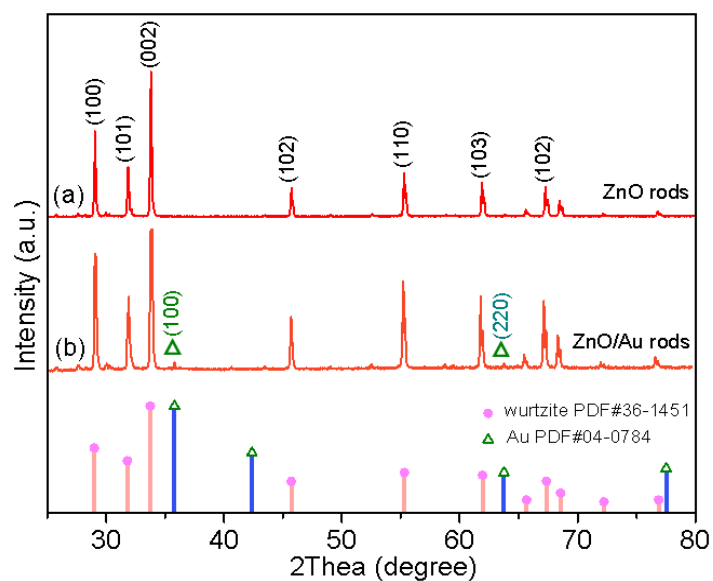
Figure S2. XRD patterns of the (a) ZnO rods and (b) ZnO/Au rods. For the Janus ZnO/Au rods, a dividing line between Au region (bright) and ZnO region (dark) along the major axis of the rod can be observed in the SEM image (Figure S3a).
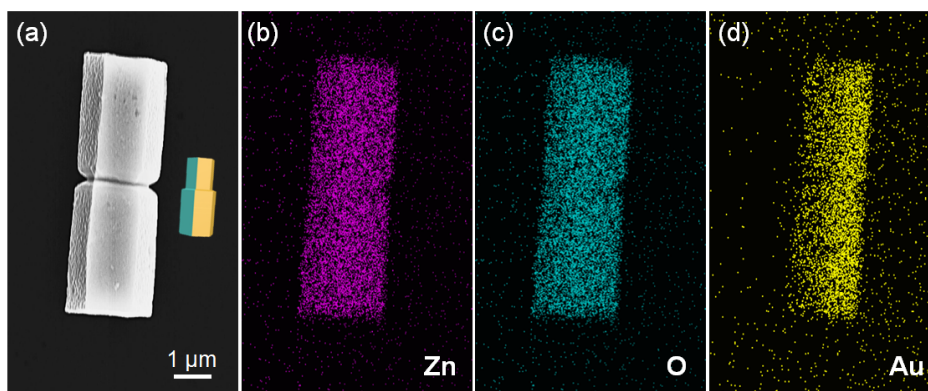

Figure S3. Energy dispersive X-ray (EDX) analysis of the ZnO/Au rod. (a) SEM image and a schematic of the rod, (b-d) the corresponding EDX mapping images for elements Zn, O, Au, respectively.

2.2 The self-electrophoresis mechanism

To further validate the self-electrophoresis mechanism, control experiments of the ZnO/Au rods in NaCl aqueous solution were conducted. As shown in the Figure S4, the velocities, v and ω, of the rod decrease dramatically with increasing NaCl concentration. And no motion is detectable for rods in 10 mM NaCl solution. These results are consistent with the theory of electrokinetic motion, and confirm the self-electrophoresis mechanism as previously reported for spherical micromotors.[3-4]
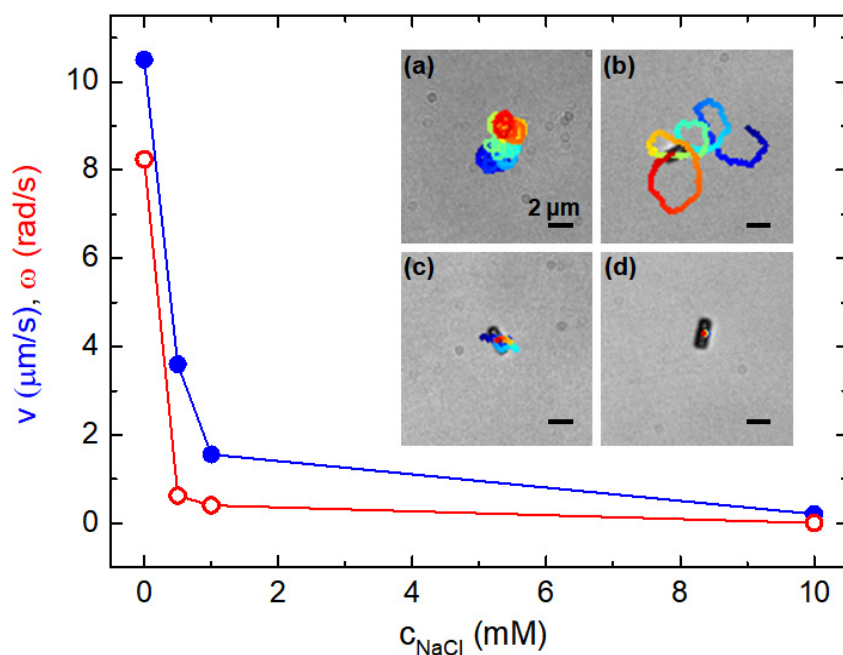

Figure S4. Linear velocity (v) and angular velocity (ω) of the motion of ZnO/Au rods as a function of the NaCl concentrations in presence of 1% H_2O_2 and with UV light intensities of 32 mW/cm^2. The corresponding trajectories at those NaCl concentrations are presented in the inset: (a) 0 mM; (b) 0.5 mM; (c) 1.0 mM; and (d) 10 mM. Scale bars: 2 μm.

2.3 The intensity of the UV light affects the motion modes

We further studied the effect of the UV light intensity on the motion modes. As shown in the Figure S5, with increasing UV light intensities, tight, circular trajectories are observed, indicating the rods switch modes from ballistic motion to circular motion. The effect of adjusting light intensities on the motion mode is thus similar to the effect of adjusting the fuel concentrations (Figure 2 of the *main text*).
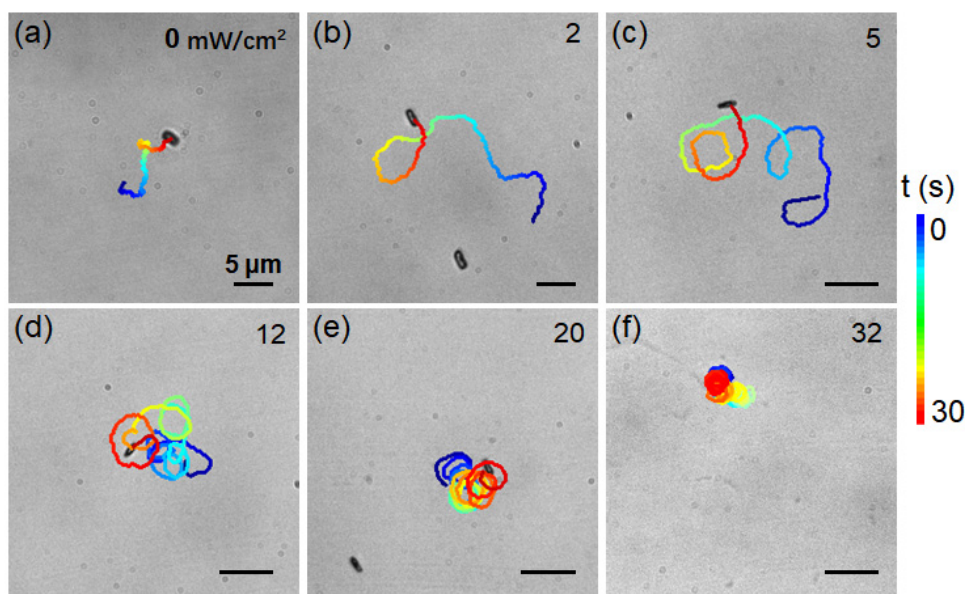

Figure S5. Effect of UV light intensities on the motion modes of ZnO/Au rods. Representative trajectories of the rods moving in 1% H_2O_2 solution with increasing UV light intensities: (a) 0 mW/cm^2; (b) 2 mW/cm^2; (c) 5 mW/cm^2; (d) 12 mW/cm^2; (e) 20 mW/cm^2; and (f) 32 mW/cm^2. Scale bars: 5 μm.

2.4 More characterizations on rotational motion

The ZnO/Au rod has no preferred directions of rotation, and we found the direction is approximately 50% clockwise and 50% counterclockwise after examining 110 rods undergo rotational motion. The trajectory radii are inversely related to fuel concentrations (Figure S6c), while the rotational diffusion coefficients are proportional to the fuel concentrations (Figure S6d).
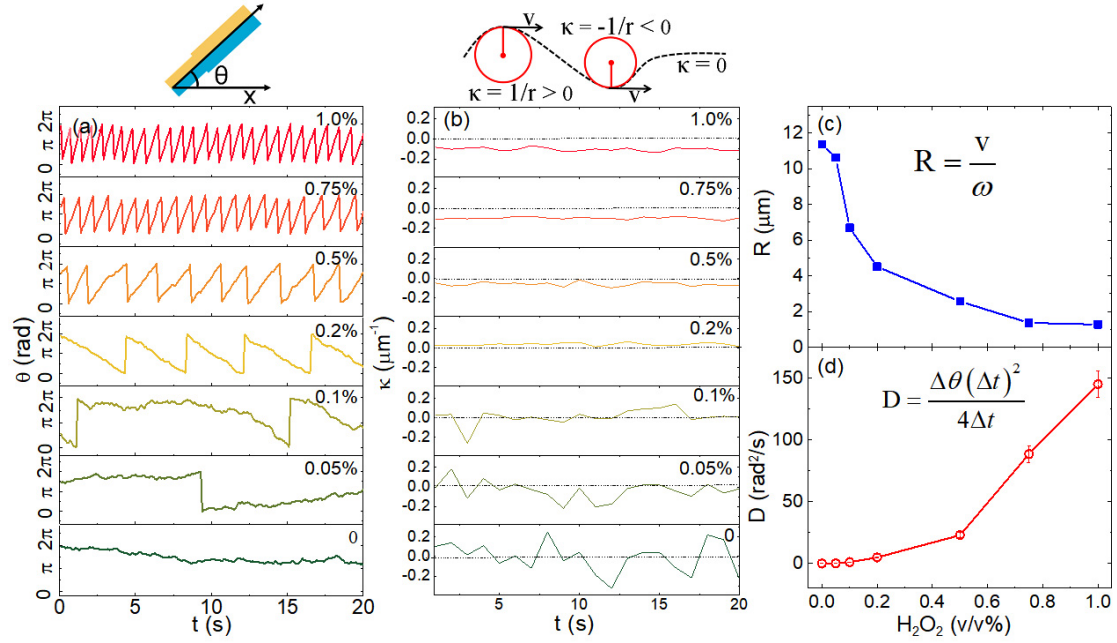
Figure S6. Effect of H_2O_2 concentrations on the motion of the ZnO/Au rod. (a) Angle, θ; (b) curvatures, κ; (c) trajectory radius, R; and (d) rotational diffusion coefficient, D, for the ZnO/Au rod in various H_2O_2 concentrations.

2.5 The geometric asymmetry of the ZnO/Au rod dictates the motion modes: twinned rods vs. uniform rods
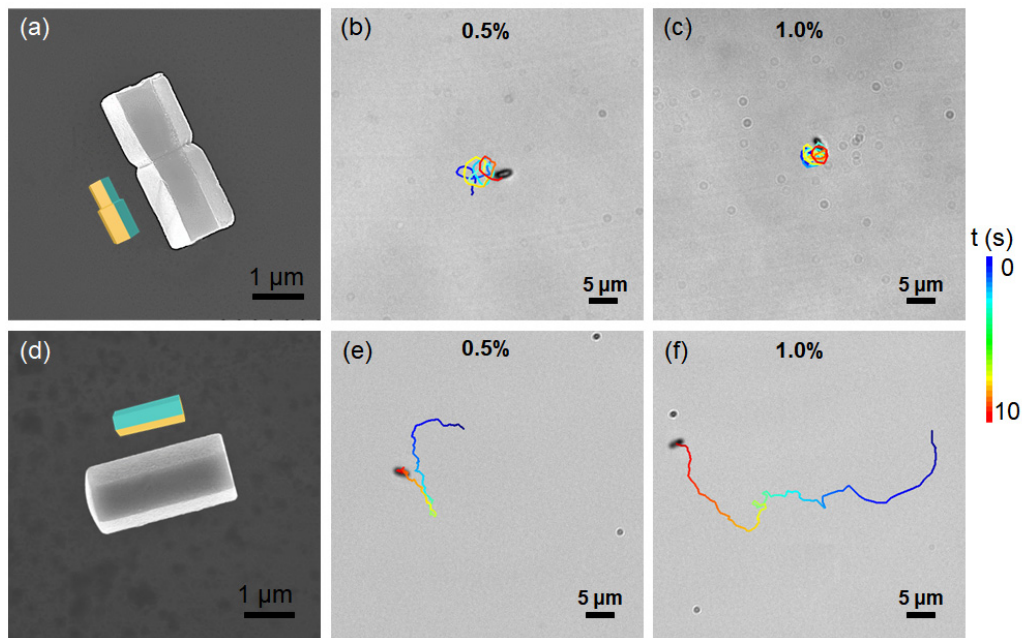

Figure S7. The geometric asymmetry of the ZnO/Au rod dictates the motion modes. Top row: (a) SEM image of the twinned ZnO/Au rod, (b) and (c) twinned rods undergo *rotation-dominated* motion in 0.5% and 1.0% H_2O_2 solutions. Bottom row: (d) SEM image of the uniform Janus ZnO/Au rod, (e) and (f) uniform rods undergo *translation-dominated* motion in 0.5% and 1.0% H_2O_2 solutions.

2.6 Cargo loading and release

When the ZnO/Au rod is exposed to UV irradiation, electrons in ZnO received energy from the photons and are excited to the conduction band (CB).[3, 4] Such photo-excited electrons prefer to trapped into Au layer because Au with lower Fermi levels can act as an electron sink.[4] Therefore, negative charges built on the Au side while positive charges built on the ZnO side. Thus the positively charged side captures the negatively charged cargos via electrostatic attraction.[5, 6] When the UV irradiation is off, no fresh electron-hole pairs are photo-generated in the rod.[4] In this case, both the ZnO and the Au sides are negatively charged, leading to the release of the negatively charged cargos due to electrostatic repulsion.[5, 6]
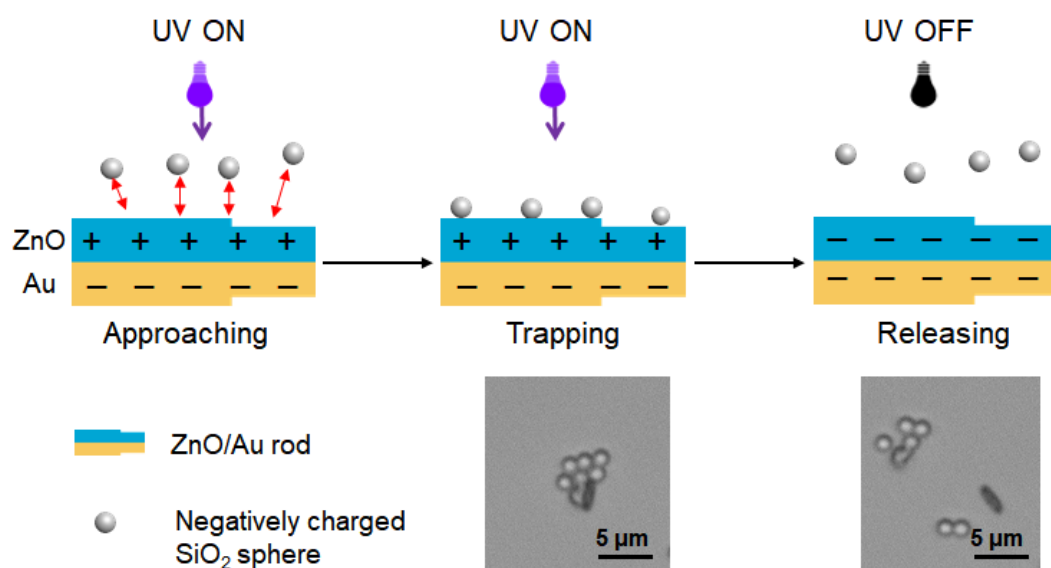

Figure S8. Schematic diagram and optical micrographs of a ZnO/Au rod approaches, captures and releases cargos.
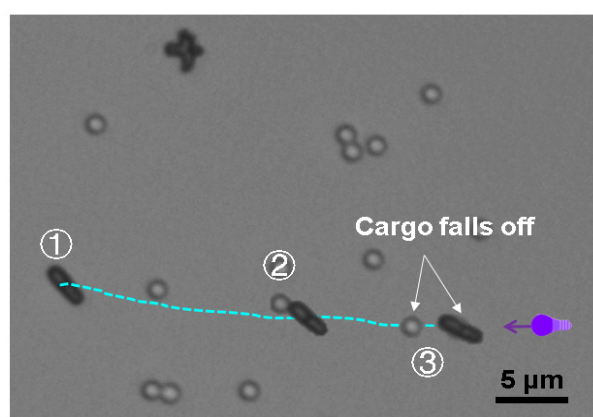

Figure S9. A ZnO/Au rod loses its cargo during translational motion. ①approaches, ② captures, and ③cargo falls off during the transportation process.

3. Materials and Methods

3.1 Materials

All the reagents were analytical grade and used without further purification. Zinc nitrate hexahydrate ($Zn(NO_3)_2·6H_2O$) was purchased from Shandong XiYa Chemical Industry Co., Ltd. Sodium hydroxide (NaOH), and hydrogen peroxide (H_2O_2) were obtained from Sigma-Aldrich (Shanghai) Trading Co., Ltd.

3.2 Synthesis of ZnO rods

The ZnO rods were large-scale synthesized by a hydrothermal method according to a previously report method.[1] Briefly, an aqueous solution of NaOH (1.5 M) was added dropwise to a well-stirred $Zn(NO_3)_2·6H_2O$ aqueous solution (0.5 M) to form white slurry. Then the resulting slurry was transferred into a 50 mL Teflon-lined stainless steel autoclave and kept 150 ℃ for 12 h. The final products were washed with distilled water and absolute ethanol, and then dried in air at 60 ℃ for 12 h.

3.3 Preparation of ZnO/Au rods

To fabricate the ZnO/Au rod, a monolayer of ZnO rods was first formed on a glass slide by suspension casting. Then the monolayer of the rods was coated with a thin layer of Au by sputtering with a Q150T metal sputter (Quorum Technologies). Finally, the ZnO/Au rods were collected by sonication in ethanol and washed three times with distilled water.

3.4 Finite Element Modeling

The distribution of electric and fluid flow fields around a ZnO/Au rod were calculated by finite element simulation (COMSOL Multiphysics, version 5.2a). The simulation model is shown in Figure S10.
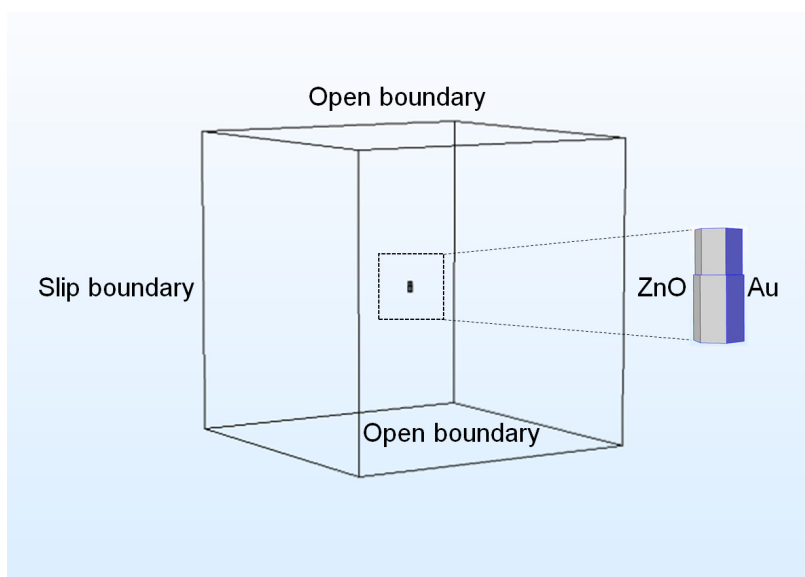

Figure S10. Schematic diagram of a 3D ZnO/Au rod model used in the simulation.

One segment of the ZnO/Au rod is 0.75 μm on each side and 1.9 μm in length, whereas the other segment is 0.7 μm on each side and 1.3 μm in length. The ZnO/Au rod was placed in the center of a cube with 100 μm on per side which is filled with water containing saturated CO_2. The top and bottom of the box were set to be open boundary for the flow, while the side walls were slip boundaries (no stress). And the fluid was set as incompressible flow to simulate the Stokes flow. The flux was set to be 7×10^{-6} mol/m^2·s. In this model, a nonlinear steady solver is carried out to calculate the distribution of electric and fluid flow field.

Since the particle is fixed in space and fluid flows freely, we are essentially modeling the particle motion in the reference frame of the particle itself. The electrostatic module and creeping flow module were the physics used in building the model. The two modules are coupled by an electro-osmotic boundary condition on the particle surface.

In electrostatic modules, one side simulates ZnO (anode) with an outward flux of protons and carries a surface charge density (ρ_{ZnO}) by,

$$\rho_{ZnO} = \varepsilon E_{ZnO} = \varepsilon \frac{J k_B T}{2 e n_0 D_{H^+}} \tag{1}$$

Where ε is the medium electrical permittivity and n_0 is the bulk proton concentration. J is the ionic flux, D_{H^+} is the diffusivities of H^+.

The other side simulates the Au with an inward flux of the same magnitude of the anode and carries an opposite surface charge density (ρ_{Au}) by,

$$\rho_{Au} = \varepsilon E_{Au} = \varepsilon \frac{-J k_B T}{2 e n_0 D_{H^+}} \tag{2}$$

The solution is saturated with ambient atmospheric CO_2 and the first dissociation of carbonic acid is considered to be the equilibrium. Proton bulk concentration are calculated as $n_0 = 2.24 \times 10^{-3}$ mol/m^3.

In creeping flow, there is an electroosmotic boundary condition on the particle surface:

$$v = \frac{\zeta \varepsilon}{\mu} E \tag{3}$$

where v is the electroosmotic speed of fluid on the particle surface, ζ is the zeta potential on the particle surface, E is the tangential component of the electric field.

3.5 Characterizations of ZnO/Au Rods

The morphology of the ZnO rod and the ZnO/Au rod were examined by Scanning Electron Microscope (SEM, SU8010, Hitachi). X-ray diffraction (XRD) data were collected on a Holland Panalytical X'Pert Pro MPD X-ray diffractometer to evaluate the crystallinity of the rods. The Zeta potentials were measured on a Malvern Zetasizer NanoZS to determine the surface charge of the rods.

3.6 Optical Video Microscopy

The motion of ZnO/Au rods were observed and recorded at 10 frames per second by a Basler ACE camera fitted on a Zeiss Observer A1 microscope. For microscopy samples, the rods were dispersed in H_2O_2 solutions and the dispersion was loaded in a simple rectangular inspection chambers made of glass slides and epoxy glue. The motion of the rods was triggered by a compact UV light with of a wavelength of 365 nm and a maximum power intensity of 32 mW/cm^2. To study the effect of H_2O_2 concentrations on the motion modes of ZnO/Au rods, the concentrations were varied systemically from 0 to 1.0 %. To study the effect of the orientation of the incident light on the motion modes, UV lights were setup on the microscope stage to achieve the desired incident angles.

3.7 Analysis of the Motion of ZnO/Au Rods.

The ZnO/Au rods in optical micrographs were identified by image analysis using Image J (NIH), to obtain the rods' positional coordinates, x and y, as well as their orientation angles, θ. The positional and orientation data were further analyzed using in-house computer programs written in IDL (Exelis) to calculate translational velocity (v), angular velocity (ω), trajectory curvature (κ), and mean-square angular displacement ($<\Delta\theta^2>$) of the rods.

Supplementary References

1. Kiomarsipour, N.; Shoja Razavi, R., Characterization and optical property of ZnO nano-, submicro- and microrods synthesized by hydrothermal method on a large-scale. *Superlattice. Microst.* **2012**, *52*, 704-710.

2. Sarkar, S.; Makhal, A.; Bora, T.; Baruah, S.; Dutta, J.; Pal, S. K., Photoselective excited state dynamics in ZnO-Au nanocomposites and their implications in photocatalysis and dye-sensitized solar cells. *Phys. Chem. Chem. Phys.* **2011**, *13*, 12488-12496.

3. Dong, R.; Zhang, Q.; Gao, W.; Pei, A.; Ren, B. Highly Efficient Light-Driven TiO$_2$-Au Janus Micromotors. *ACS Nano* **2016**, *10*, 839-844.

4. Paxton, W. F.; Baker, P. T.; Kline, T. R.; Wang, Y.; Mallouk, T. E.; Sen, A. Catalytically Induced Electrokinetics for Motors and Micropumps. *J. Am. Chem. Soc.* **2006**, *128*, 14881-14888.

5. Mou, F.; Kong, L.; Chen, C.; Chen, Z.; Xu, L.; Guan, J. Light-controlled propulsion, aggregation and separation of water-fuelled TiO$_2$/Pt Janus submicromotors and their "on-the-fly" photocatalytic activities. *Nanoscale*, **2016**,*8*, 4976-4983.

6. Wang, W.; Duan W.; Sen A.; Mallouk, T. E. Catalytically powered dynamic assembly of rod-shaped nanomotors and passive tracer particles. *PNAS* **2013**, *110*, 17744-17749.